

Epidemics as an adaptive driving force determining lifespan setpoints

Supplementary Materials.

Peter V. Lidsky¹ and Raul Andino¹

Department of Microbiology and Immunology, University of California, 600 16th Street, GH-S572, UCSF Box 2280, San Francisco, California 94143-2280, USA.

¹ Corresponding authors

Methods.

All scripts were coded in Python 2.7 (Python Software Foundation). Generation of uniformly distributed random numbers in all cases was performed with the *random* Python library, which uses a standard Mersenne Twister algorithm. Differential equations were analyzed with the *odeint* function of the *scipy* library. Data were plotted with *matplotlib* and *seaborn* python packages and with Excel (Microsoft).

Model I. Length of lifespan controls epidemics establishment and progression.

Stochastic model.

Map. To investigate the effects of lifespan on pathogen spread, we modeled a spatially distributed population of individuals. The area occupied by the experimental population was a square with the side of 10^4 length units (l.u) To avoid border effects, the individuals were moving across borders in a way that an individual moving, for example, beyond the right limit of the coordinate axis reentered the field from the left border of the map. All other interactions were also calculated across the borders, and the experimental space was thus behaving as a surface of a toroid with negligible curvature.

Movement. The stochastic movement of individuals was simulated. The speed of each individual was set to be 100 l.u. per time unit (t.u.). Individuals were programmed to change the direction of their movement randomly with a probability of 0.1 per t.u.

Infection was simulated in the following way. If an infected individual approached a susceptible one, the susceptible individual became infected with the probability of $\beta \cdot \frac{d_{\max}^2 - d^2}{d_{\max}^2}$, where β was the transmission efficiency (an intrinsic property of the pathogen), d was the distance between individuals and d_{\max} was a maximum distance of pathogen diffusion. d_{\max} was set to be 200 l.u. in all the simulations performed. No effects of infection on fitness were considered in Figures 1, 2, and 3.

Pathogen reintroduction. If the number of infected individuals went below 10, additional random hosts were changed to be infected. Thus, the pathogen could not be completely lost from the population.

Age and death. The age (g) of each individual was incremented by 1 each t.u. Mortality was calculated based on age. In Fig. 1, mortality was sharply set at the age of the lifespan setpoint (A_{\max}). Thus, mortality was 0 at ages $g < A_{\max}$ and 1 at $g \geq A_{\max}$.

In Fig. S1C (Type I survivorship curve), the probability of death at a given age was calculated with Gompertz's equation: $M_a \cdot e^{M_b \cdot t}$, where M_a was the age-independent component of mortality set to 10^{-6} , and M_b was an age-dependent component and variable. In Fig. S1E (Type II survivorship curve), the mortality was constant across all ages of an individual and was defined as M_a .

Host reproduction was simulated in the following way. At each timepoint, a value was added to the replication value ($W_{t+1} = W_t + f \cdot B$), where f was the physiological fitness of the individual and B was the birth rate. The fitness of a healthy animal was set to $f = 100$. If W exceeded the threshold value, a

new individual was born in the vicinity of the parent individual, and W of both was set to 0. The value of the threshold was defined as 100. For example, if $B = 0.05$, the individual will deliver its first progeny at the age of 20 ($20 \cdot B \cdot f = 20 \cdot 0.05 \cdot 100 = 100$) and then at ages 40, 60, 80, and so on. In Figures 1 and S1, birth rate was set to be $B = 0.4$, a high value ensuring a constant maximum number of individuals in experimental niches. Reproduction was asexual, and the genotype of the progeny was always an exact copy of parent's.

Pathogen penalty on reproduction. In Figures 4, 5, 6, and 7, the pathogen was set to have a negative effect on replication. In this case, fitness was calculated as $f = 100 \cdot (1 - P)$, where P was the pathogen penalty on fitness ($0 \leq P \leq 1$).

Population control in this model was a sharp restriction of population number by $N_{\max} = 5000$ maximum individuals. If an individual was to deliver progeny in a population with a number of N_{\max} , that progeny was considered to be expelled or aborted. The parent's W in such a situation was still set to zero.

The order of an individual's analysis can create biases. To avoid that, the order of the individual's analysis was randomized at each timepoint in all simulations.

Data collection. In Figures 1C, S1C and S1E, pathogen prevalence was estimated after the equilibrium between infected and uninfected hosts was reached. The criteria of the equilibrium were: (i) the overall time of simulation was more than 1000 t.u. and (ii) the mean pathogen load in a time interval [-1000, -500] was higher or equal to that in the interval [-500, 0]. The simulation was run for different values of A (interval [30, 300] with the step of 15) and β (interval of [0, 0.03] with the step of 0.0005).

Calculation of R_0 . To make an estimate demonstrated in Figure 1D, the actual transmission rate β^* was calculated. β^* directly depended on β and had a component related to the spatial effects of infection. To find β^* , we used a population of 5000 individuals with 50 of them infected. We collected the number of newly infected hosts at different values of β . Each value of β in an interval [0, 0.03] with a step size of 0.0005 was analyzed in 100 replicates. We found β^* linearly depended on β : $\beta^* \approx \beta \cdot 3.2744$. We used this coefficient to produce a graph in Figure 1D.

Model II. Zoonotic transmission, pathogen adaptation and lifespan setpoints.

Stochastic model.

Pathogen passages. To investigate the effects of the lifespan on pathogen adaptation after zoonotic transmission, we performed the modeling as above, except that each infected host had an additional parameter: the passage of the pathogen. Initial infections and new infections (if the number of infected hosts went below 10) were set to have passage 1. The individuals infected from these were assigned with passage number 2, etc. Passage number affected pathogen transmission (β). We considered early passages (< 10) to have low β_n (n for naive) due to insufficient adaptation. In later passages (≥ 10),

pathogens acquired higher transmission β_a (a for adapted). The difference between naive and adapted transmission efficiency was set to be 10-fold, $\beta_n = \frac{\beta_a}{10}$.

Data collection. The simulation was run for 5000 t.u. with different values of β_a and A_{\max} . If a pathogen with the passage number of 10 was produced, the simulation was stopped, and the time of adaptation was recorded. Simulations were run for different values of A (interval [30, 300] with the step of 15) and β (interval of [0, 0.1] with the step of 0.0005).

Deterministic model.

To corroborate the findings made in the stochastic model, we adapted the classical equations (Anderson and May, 1982) to a form:

$$\begin{cases} \frac{dI_{i(2 \leq i \leq 10)}}{dt} = -\frac{I_i}{A} + \frac{\beta_n \cdot S \cdot I_{i-1}}{N_{\max}} \\ \frac{dS}{dt} = -\frac{S}{A} + (S + \sum_{i=1}^{10} I_i) \cdot B \cdot \frac{N_{\max}^5 - (S + \sum_{i=1}^{10} I_i)^5}{N_{\max}^5} - \sum_{i=2}^{10} \frac{\beta_n \cdot S \cdot I_{i-1}}{N_{\max}} \end{cases}$$

, where S was the number of uninfected susceptible individuals, I_n was the number of individuals infected with a pathogen with passage number n , A was lifespan, β_n was the pathogen transmission of a naive pathogen, N_{\max} was the maximum carrying capacity of the niche, and B was the birth rate. The

fixed parameters were $N_{\max} = 5000$ and $B = 0.4$. The 5th powers in the component $\frac{N_{\max}^5 - (S + \sum_{i=1}^{10} I_i)^5}{N_{\max}^5}$

, responsible for the population density-dependent birth control was to simulate the sharp population limit, similar to that used in the stochastic model.

To find a domain where the pathogen can get adapted (Fig. 2C, above solid line), the initial populations were set to: $S^{t=0} = 4990$; $I_1^{t=0} = 10$; $I_{(2..10)}^{t=0} = 0$. The criterion of successful pathogen adaptation was $I_{10} > 1$ in a simulation of 50000 t.u. long.

To find the domain of feasibility, where the fully adapted pathogen cannot replicate (Fig. 2C, below dashed line), the populations were set to: $S^{t=0} = 4998$; $I_{10}^{t=0} = 2$; $I_{(1..9)}^{t=0} = 0$, and the above system was modified accordingly:

$$\begin{cases} \frac{dI_{10}}{dt} = -\frac{I_{10}}{A} + \frac{\beta_a \cdot S \cdot I_{10}}{N_{\max}} \\ \frac{dS}{dt} = -\frac{S}{A} + (S + I_{10}) \cdot B \cdot \frac{N_{\max}^5 - (S + I_{10})^5}{N_{\max}^5} - \frac{\beta_a \cdot S \cdot I_{10}}{N_{\max}} \end{cases}$$

The criterion of successful pathogen replication was $I_{10} > 1$ for at least in one-time point in the interval [25000, 50000].

Numeric differences between stochastic and deterministic models were due to the presence of spatial distribution component in pathogen transmission in the stochastic model and its absence in the deterministic model.

Model III. Short lifespan facilitates pathogens clearance during critical declines in host's density or population bottlenecks.

Stochastic model.

To investigate the effects of bottlenecks on pathogen clearance, the simulations were performed as in Model I with some modifications. First, the birth rate was set to be $B = 0.05$, since the speed of population growth has a huge impact on pathogen cleaning. Second, the simulation was started with only 25 infected individuals. Third, the pathogens were not reintroduced if their numbers were going low. Simulations were run for 3000 t.u. The criterion for pathogen clearance was the entire absence of the infected individuals. The criterion of pathogen retention in population was the presence of 100 infected individuals. Simulations were run for different values of A (interval [30, 300] with the step of 5) and β (interval of [0, 0.03] with the step of 0.0005). Each simulation was repeated for 10 times, and an average success rate of pathogen retention was calculated (Figure 3B).

Deterministic model.

To corroborate findings made in the stochastic model, we again used classical equations (Anderson and May, 1982) with modifications:

$$\begin{cases} \frac{dI}{dt} = -\frac{I}{A} + \frac{\beta \cdot S \cdot I}{N_{\max}} \\ \frac{dS}{dt} = -\frac{S}{A} + (S + I) \cdot B \cdot \frac{N_{\max}^5 - (S + I)^5}{N_{\max}^5} - \frac{\beta \cdot S \cdot I}{N_{\max}} \end{cases}$$

$N_{\max} = 5000; B = 0.02, 0.03, 0.05$. As in the case of the deterministic Model II, the 5th power in the density-related component was to simulate growth limit more closely to the stochastic model. The initial population sizes were $S^{t=0} = 0; I^{t=0} = 25$ for estimating the bottleneck effects or $S^{t=0} = 4975; I^{t=0} = 25$ for finding the domain where the pathogen is not capable to replicate in a fully populated niche. The criterion of pathogen clearance by the bottleneck was $I < 1$ at any timepoint of the simulation, and the

criterion for pathogen retention was $-I > 1$ across all span of simulation ($5 \cdot 10^4$ time points). With this setup, we readily found domains where the pathogen was feasible in fully populated niches but is cleared by dramatic declines in population density (Figure 3E). The efficiency of clearance strongly depended on A and B .

Model IV. Infection in viscous populations favors selection of short-lived hosts.

Stochastic model.

For modeling population viscosity, we simulated the mutual repulsion of individuals. We modified the Model I in the following way.

Movement and repulsion. The directionality of the individual's movement was set to depend on the neighbor's positions. At each time point, for all the neighbors of each individual within 400 l.u., the

distance was detected, and the resulting movement speed was calculated as $\overrightarrow{V}_{t+1} = \overrightarrow{V}_t + R \cdot \sum_{i=1}^n \frac{\overrightarrow{d}_i}{|d_i|^3}$,

where \overrightarrow{V} was the vector speed of the individual, R was a constant reflecting the power of repulsion, \overrightarrow{d}_i was the vector distance between this individual and i neighboring individual, and n was the total number of neighbors. Next, to limit diffusion and simulate viscosity more accurately, the maximum speed of the individual was reduced to 10 l.u./t.u. Thus, the individuals were constantly moving away from each other, forming an irregular lattice. This type of movement reflected the behavior of territorial animals or animals to optimize the availability of the resources if those are limited and spatially distributed.

Local context-based control of population density. To simulate local population control and local density gradients, we set the individual's fecundity to depend on the area the individual controls without competing with other individuals. The maximum area was set to be circular with a radius of $r = 100$ l.u.

A maximum area occupied by an individual was, therefore, $M_{\max} = \pi r^2$. The overlap between two individual areas (Fig. 5A) was calculated as $\frac{\alpha - \sin(\alpha)}{2} \cdot r^2$, where α was found as

$\alpha = 2 \cdot \arccos\left(\frac{d/2}{r}\right)$. The individual area (M) was found by subtraction of all these overlaps from

M_{\max} .

The replication was simulated in a manner, similar to model I: $W_{t+1} = W_t + 100 \cdot B \cdot \frac{M}{M_{\max}} \cdot (1 - P)$,

where B was the birth rate and P was the disease-related penalty. When W reached a threshold value of 100, a daughter individual appeared next to its parent, and the W of both individuals was set to zero. The position of the newborn individual was 1 l.u. away from the parent in a scalar. The vector position was randomized to avoid biases of the initial placement of the newborns.

The scenario of simulation and data collection. The experiments were first populated with short-lived individuals (typically $A = 90$ t.u.) with randomized ages (g) and replication values (W). Then the

pathogens were introduced: 10 random individuals were marked as infected (or see below). Next, a small group of individuals located in the middle of the field was turned into long-lived variants (typically $A = 180$ t.u.). The simulation was run until one of the two strains became entirely extinct, and the identity of this winning strain was recorded as the main output parameter.

Sensitivity analysis. To investigate the parameters affecting the competition between short-lived and long-lived strains, we determined if the initial placement of the pathogen affects the final outcome. The speed of selection depended highly on the time when the long-lived strain encountered the pathogen. If the pathogen was encountered too late (less than 1% of simulations), the long-lived strain could take over the population before the epidemics were fully developed. This effect simulated evolution with a limited number of animals (~4-6 thousand) and in a small volume. To overcome this artifact and make our simulations more uniform in terms of time, without extending the size of the simulated population, we placed four initial epidemics at a defined distance from where the long-lived strain was emerging (Fig. S2A).

With such a setup, the short-lived strain always took over the population ($n > 200$). Then we performed a sensitivity assay to find parameters that affect the outcome of the competition. We found that pathogen transmission (β), pathogen penalty (P), host's birth rate (B), the power of repulsion between individuals (R), and a ratio of lifespan of the short-lived (A_{SL}) and long-lived (A_{LL}) individuals are important for the outcome.

Since the decrease in repulsion (R) was associated with the deoptimization of the individual's territories and decrease in fitness, we used an alternative method to examine the effect of viscosity in lifespan setpoint selection. An individual that encounter other individual swapped their positions with a given probability (S). This method of modeling viscosity gave similar results to the simple decrease in repulsion (Fig. S2K, S2L, S2M).

For each of the above parameters, we performed a series of simulations with different values of β . This approach was based on an assumption that, in nature, organisms are exposed to many pathogens with different transmission rates.

We also investigated the role of vertical transmission (infection of the daughter individual by the parent immediately after the birth, Figure S2B). 50% vertical transmission moderately expanded the domain where short-lived individuals outcompeted the long-lived ones.

The results of the sensitivity analysis are shown in Fig. 6 and S6 and discussed in the text. Each datapoint is a proportion of simulations (>20 per datapoint) in which the short-lived individuals won in the competition.

Position-based labeling of individuals. To find out if the emergence of long-lived mutant affects the replication success of the neighboring short-lived individuals, in the start of the simulations, we labeled the short-lived individuals, according to the distance from the locus of the initial long-lived mutant placement. This label was then transmitted from each individual to its progeny. Thus, at the end of the simulation, we could score the relative reproductive success of the individuals as a function of its ancestor's initial position. To produce the graphs presented in Fig. 7D, we obtained data from 50

independent simulations with random initial pathogen placement. In the case of the complete experimental scenario of selection, data were collected after the long-lived mutant was eliminated. In control simulations (a scenario without long-lived mutant emergence or a scenario without both long-lived mutant and the pathogen), data were collected after $3 \cdot 10^3$ time points. This timeframe was comparable to the time of the long-lived strain extinction. The extracted inherited positions were separated into 100 bins, according to the distances, and the number of individuals in each bin was normalized for the average number of individuals in that bin by the time of simulation started. The obtained curves were smoothened with the smoothening factor of 20 and plotted.

Deterministic model.

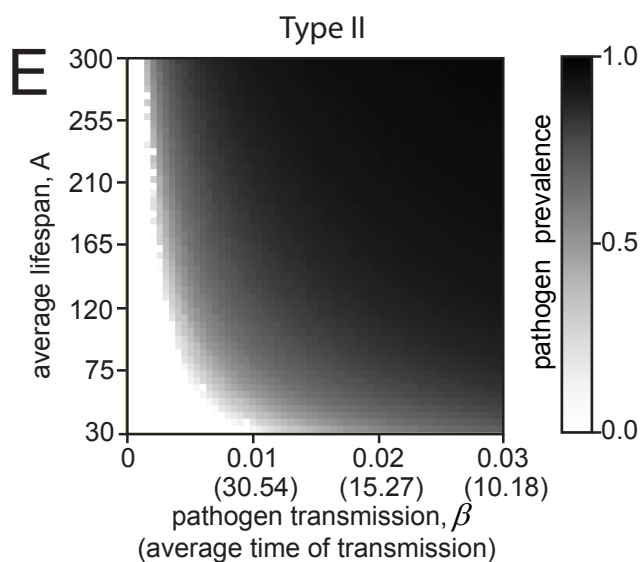
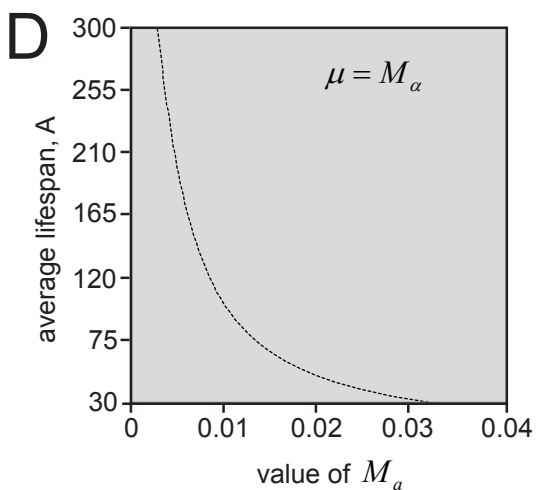
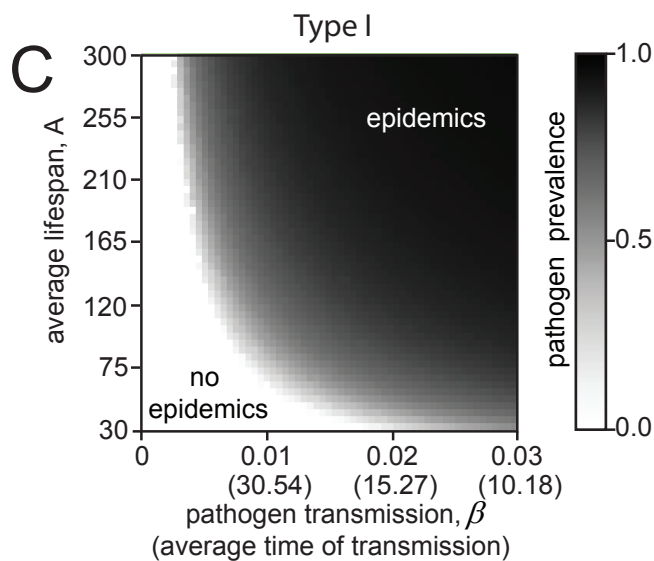
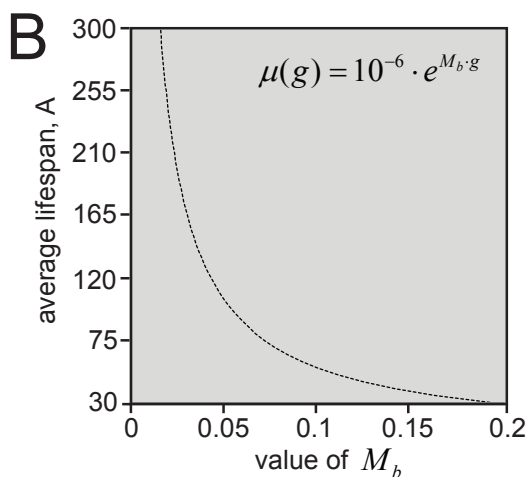
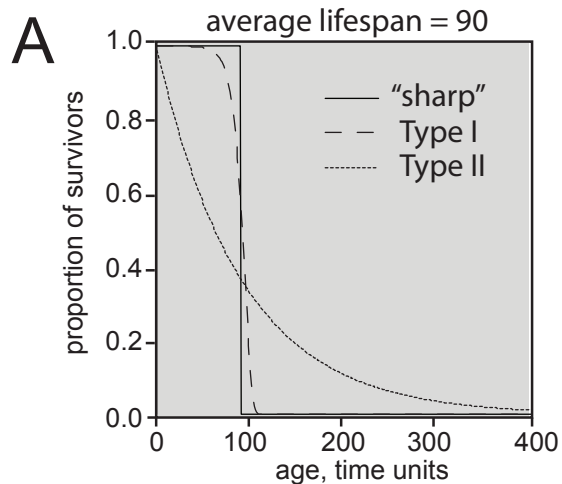
This model is described in the main text.

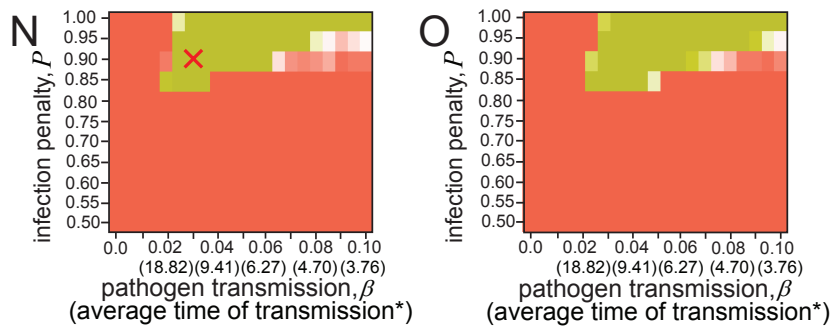
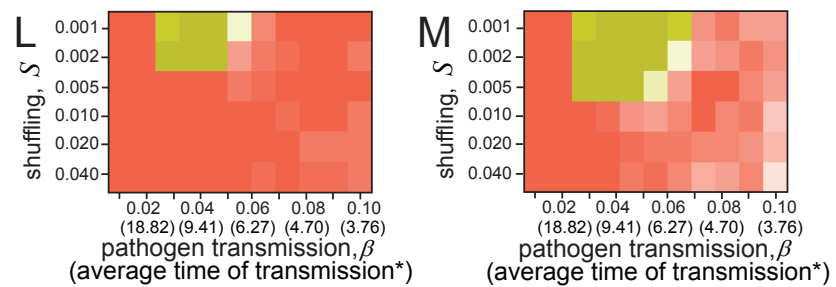
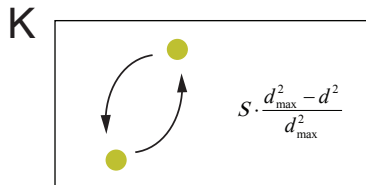
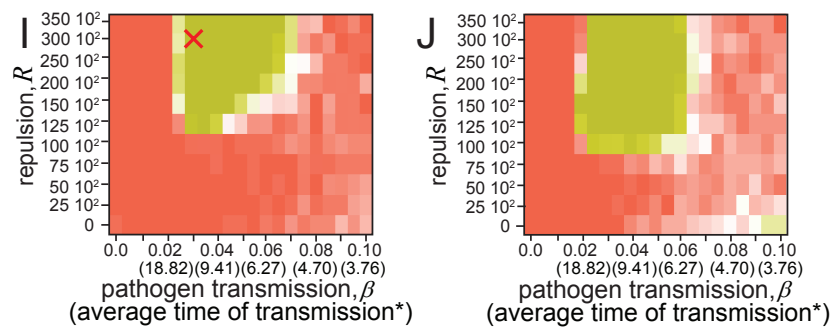
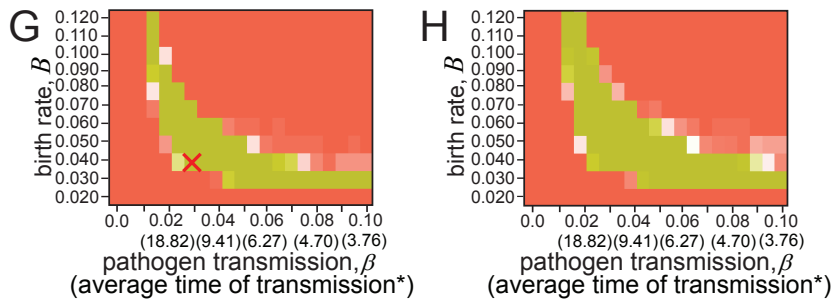
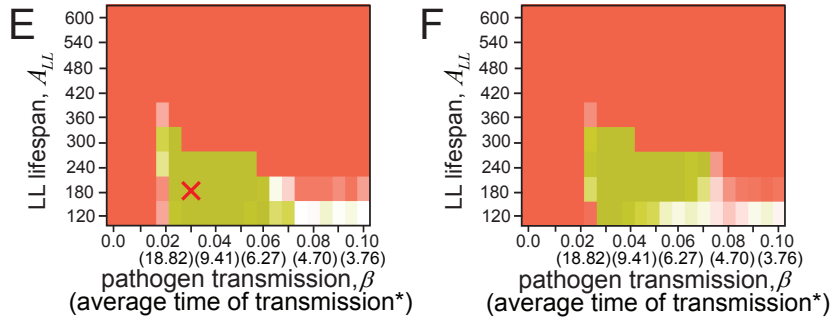
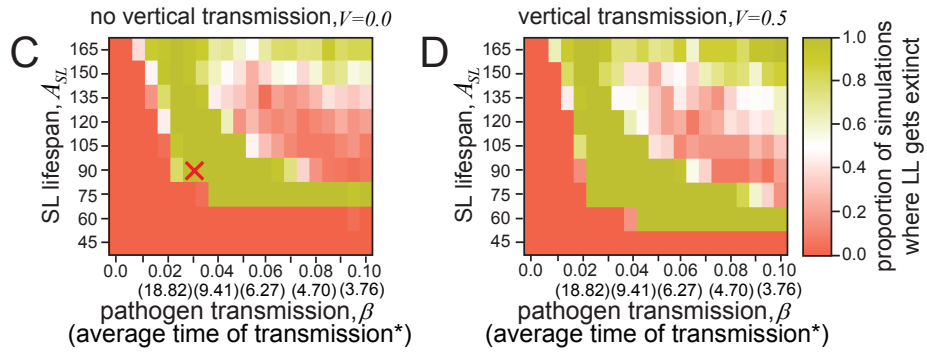
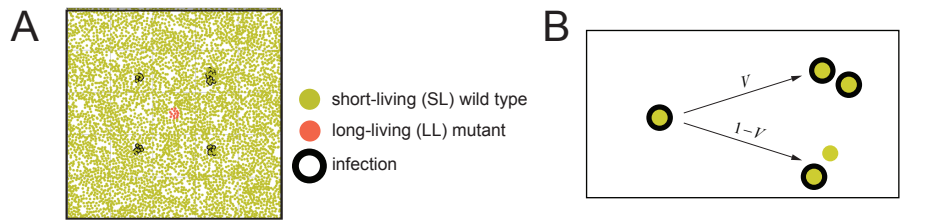
Supplementary references

Anderson, R.M., and May, R.M. (1982). Coevolution of hosts and parasites. *Parasitology* 85 (Pt 2), 411-426.

Deevey, E.S. (1947). Life Tables for Natural Populations of Animals. *The Quarterly Review of Biology* 22, 283-314.

Jones, O.R., Scheuerlein, A., Salguero-Gomez, R., Camarda, C.G., Schaible, R., Casper, B.B., Dahlgren, J.P., Ehrlén, J., Garcia, M.B., Menges, E.S., *et al.* (2014). Diversity of ageing across the tree of life. *Nature* 505, 169-173.





Supplementary Figure Legends

Fig. S1. Related to Fig. 1. The shapes of mortality curves do not strongly affect the susceptibility of populations to infections. **A.** The examples of three survivorship curves. “sharp” stands for an immediate death of the individual upon reaching an age of lifespan setpoint. The type I survivorship curve is a characteristic of many large mammals (Deevey, 1947; Jones et al., 2014) and implies a significant growth of mortality with age. Mortality dependence on age (g) was calculated, according to the Gompertz’s equation $\mu(g) = M_\alpha \cdot e^{M_\beta \cdot g}$ with mortality parameters $M_\alpha = 10^{-6}$ and $M_\beta = 0.0582$. Type II survivorship is typical for many smaller animals and implies a higher mortality that does not depend on age, $M_\alpha = 0.011$; $M_\beta = 0$. The average individual’s lifespan with all three life histories shown in this panel was 90 t.u. **B.** Finding the values of M_β that correspond to the average lifespans of the individuals as in Figure 1C if $M_\alpha = 10^{-6}$. **C.** Pathogen prevalence in populations of individuals with Type I survivorship curve and average lifespans as in Fig. 1C. Average time of transmission (in parenthesis) was estimated experimentally as an average time required for a single infected host to infect a single susceptible host in uninfected population. It is expressed in the same units as lifespan (A). **D.** Finding the values of M_α that correspond to the average lifespans of the individuals as in Fig. 1C if $M_\beta = 0$. **E.** Pathogen prevalence in populations of individuals with a Type II survivorship curve and average lifespans as in Fig. 1C.

Fig. S2. Related to Fig. 6. Model IV. Sensitivity analysis. **A.** Scheme of the initial pathogen placement to achieve better reproducibility. **B.** Vertical transmission. Infected parent passes the infection on to its kin with probability of V . $V=0$ in panels **C, E, G, I, L,** and **N** and $V=0.5$ in panels **D, F, H, J, M, O.** **C. –J.** and **L.–O.** Systematic analysis of parameters affecting the outcome of the competition between the long- and short-lived strains. The red crosses mark the default combination of parameters are: $\beta = 0.03$, $A_{SL} = 90$, $A_{LL} = 180$, $P = 0.9$, $B = 0.04$, $R = 3 \cdot 10^4$, $V = 0$, $S = 0$. Panels **C, E, G, I,** and **N** are equivalent to those shown in Fig. 6 and are dubbed here for the convenience of comparison.

K. Shuffling method allows decreasing population viscosity without affecting overall reproduction due to area deoptimization. Two individuals swap their positions in a distance-dependent manner.

Average time of transmission (in parenthesis) was estimated experimentally as the average time required for a single infected host to infect a single susceptible host in uninfected population. It is expressed in the same units as lifespan (A).

Movies

Movie 1. Related to Fig. 1 and S1. Pathogen prevalence with different average lifespans and different types of mortality. Movies are typical results of simulations from Fig. 1C, S1C, S1E. In each part of the movie, the average lifespans of modeled populations are 45, 90 and 135 t.u. The parameters of the Gompertz’s mortality function $\mu(g) = M_\alpha \cdot e^{M_\beta \cdot g}$ are shown above the corresponding panels. The lower

panels are the demographic pyramids. Size of the age bins is 1 t.u. Individuals of different ages are shown with colors, from green (young) to yellow (old). Infected individuals are outlined with black.

Movie 2. Related to Fig. 2. Pathogen adaptation is affected by lifespan. Typical simulations from Fig. 2B. Transmission efficiency is $\beta_n = 0.007$; $\beta_a = 0.07$. The histograms in the bottom show the pathogen distribution between different passages. In the panel with a short lifespan (45 t.u., left panel), the pathogen cannot become adapted within the simulation time (1000 t.u.) At the same time, a well-adapted pathogen (right panel) efficiently propagates in a population consisting of individuals with a lifespan of 45 t.u. Infected individuals are outlined with colors, corresponding to their passages.

Movie 3. Related to Fig. 3. Population bottleneck might result in pathogen clearance, effects of A and B . Typical simulation result from Fig. 3B. Transmission efficiency is $\beta = 0.018$. 25 infected individuals survived the bottleneck.

Movie 4. Related to Fig. 4. Invasion of long-lived mutants in short-lived uniformly mixed populations occurs independently of the pathogen presence. Short-lived individuals ($A_{SL} = 90$) are labeled with yellow, and long-lived ones ($A_{LL} = 180$) with red. Infected individuals are outlined with black. The lines in lower panels are labeled with the same colors.

Movie 5. Related to Fig. 5. The general scheme of individual's movement and population control in viscous populations. Map size was reduced to 1000x1000, and the starting number of individuals to 50. Individuals were labeled with the colors, according to their ages essentially as in Movie 1.

Movie 6. Related to Fig. 5. Epidemics and long-lived mutant expansion in viscous populations. Individuals of short 90 t.u. (yellow) and long 180 t.u. (red) lifespans. Infected individuals are outlined with black. Transmission efficiency was $\beta = 0.03$. Note that the epidemics in long-lived variant population (central panel) expand faster than the long-lived variants in a population of the short-lived individuals (right panel).

Movie 7. Related to Fig. 5. Long-lived mutants are displaced in the infected viscous population. The parameters used by default in all simulations were: $\beta = 0.03$, $P = 0.9$, $B = 0.04$, $R = 3 \cdot 10^4$.

Movie 8. Related to Fig. 6D. Coinfection with several pathogens in short-lived and long-lived strains and displacement of long-lived variants with the cumulative effect of several pathogens. Four pathogens with $\beta = 0.03$ and $P = 0.4$ were simulated for all three scenarios. Lines in lower panels show the population numbers. Histograms show the proportion of individuals infected with one (light blue), two (blue), three (dark blue) or four (black) pathogens. All the other parameters were as in Movie 7.

Movie 9. Related to Fig. 7. The emergence of the long-lived mutant is detrimental to surrounding short-lived individuals, "paternal strain". Simulations were run essentially as in Movie 7 in the absence (left) and in the presence (right) of the long-lived mutant outbreak. The short-lived individuals in the vicinity of the locus of the mutant introduction were labeled with brown. No other differences between these individuals and other short-lived individuals (yellow) were used. Black lines in lower panels show the number of infected individuals. Histograms are showing the classes colored as in the upper panels.